International Communications in Heat and Mass Transfer 126 (2021) 105351

Contents lists available at ScienceDirect

International Communications in Heat and Mass Transfer

journal homepage: www.elsevier.com/locate/ichmt

Nonlinear thermally radiative heat transport for brinkman type micropolar nano-material over an inclined surface with motile microorganisms and exponential heat source

Ying-Qing Song [a], Hassan Waqas [b], Shan Ali Khan [b], Sami Ullah Khan [c], M. Ijaz Khan [d], Yu-Ming Chu [e,f,*], Sumaira Qayyum [g]

[a] College of Science, Hunan City University, Yiyang 413000, PR China
[b] Department of Mathematics, Government College University Faisalabad, Layyah Campus, 31200, Pakistan
[c] Department of Mathematics, COMSATS University Islamabad, Sahiwal 57000, Pakistan
[d] Department of Mathematics and Statistics, Riphah International University I-14, Islamabad 44000, Pakistan
[e] Department of Mathematics, Huzhou University, Huzhou 313000, PR China
[f] Hunan Provincial Key Laboratory of Mathematical Modeling and Analysis in Engineering, Changsha University of Science & Technology, Changsha 410114, PR China
[g] Department of Mathematics, Quaid-I-Azam University, 45320, Islamabad 44000, Pakistan

ARTICLE INFO

Keywords:
Micropolar nanofluid
Microorganism
Brinkman effect
Temperature dependent heat source/sink
Exponential space-based heat source
Shooting algorithm

ABSTRACT

The novel aim of current analysis is to identify the characteristics of Arrhenius activation energy and nonlinear thermal radiation in bio-convective brinkman type micropolar nanofluid flow with gyrotactic motile microorganisms and melting phenomena through a stretched surface. The temperature dependent heat source/sink and exponential space-based thermal source are considered. Further, concentration of nano-materials and thermal fields are considered in the occurrence of Brownian motion and thermophoresis diffusion. The narrating boundary layer flow equations of brinkman type micropolar fluid model are reframed on the form of ordinary ones with the help of appropriate similarity transformation. The bvp4c collocation technique is used in the transformed model with shooting scheme to obtain a numerical solution of the original problem. The numerical data for the velocity, thermal and solutal fields, and microorganism's field is graphically designed and impacts of the prominent parameters are described in detail. It is notice from the current study velocity of fluid has diverse nature against magnetic parameter. Growing behavior of velocity field is depicted for higher estimation of mixed convection parameter. The microorganism field is boosted up by increasing melting parameter. The current model is applicable in nanotechnology, biotechnology, drug delivery, protein chips, DNA chips, food processing, cancer treatment, smart sensors and in many more fields

1. Introduction

The word “nanofluids” describes the suspension nanoparticles in the conventional fluid that are used to improve the mixed heat and mass transmission phenomena. Nanoparticles comprehension has developed the attention of scientists in recent decades owing to the significance of biomedicine, food manufacturing, electronics, biomaterials and mechanical technologies. In addition, specific cancer treatment theories, controlled drug delivery, nano-materials, fermentation engineering as well as chemotherapy are also highly dependent on the motion of the corresponding nanoparticles in the specified systems. The principle of nanofluids has been created to solve this problem. Nanofluid consisting of nanoparticles of (nanometer size) 1–100 of these materials (atoms) can boost heating efficiency and thus tend to enhance the rate of heat transportation. The thermophysical characteristics of traditional fluid are improved thru the accumulation of nanoparticles by Choi [1]. Nanofluids have many applications in industrial technology, heat control devices, chemicals industries, energy storage, energy production as well as cooling technologies. Buongiorno [2] provided analysis on nanoparticles by presenting a model for the study of the heat properties of continuously phase fluids. Ibrahim et al. [3] investigated the effect on Williamson and rate type nanofluids of viscous dispersion, melting, or chemical processes throughout an expanding surface enclosed in porous Media. Sinha et al. [4] explored the Magnetohydrodynamic heat and

* Corresponding author at: Department of Mathematics, Huzhou University, Huzhou 313000, PR China.
E-mail address: chuyuming@zjhu.edu.cn (Y.-M. Chu).

https://doi.org/10.1016/j.icheatmasstransfer.2021.105351

Available online 28 May 2021

mass transfer nanofluid stagnation-point flowing corresponding to the stretched sheet. Roşca et al. [5] exemplified the continuous mixed convective stagnation point of a water based nanofluid with a 2nd-order slip effects. Nayak et al. [6] discovered the mathematical method to the problem of the effect of relaxation and retardation viscoelastic dissipation as well as chemical processes on the distribution of Oldroyd-B nanofluids via Riga plate. Mabood et al. [7] analyzed the performance of hybrid nanofluids on distinct physiological quantity in a water-based hybrid nanoliquid included in a continuous and sufficiently developed forced convection flowing produced throughout a stretching sheet. The molecular phenomena approach is utilized to analyze the atomic activity of water based hybrids nanofluids with in a micro - channels is addressed by Arjmandfard et al. [8]. Many researchers that work on the flow of nano fluid with interesting applications in different industrial and manufacturing phenomenon see in [9–13]. Yashkun et al. [14] scrutinized the heat transport properties of the Magnetohydrodynamic nanofluid (water based) via the linear expanding and shrinking sheet in the absence of convection and thermal Radiative impacts. Ahmed et al. [15] introduced the mathematical model of unstable MHD non-Newtonian nanoliquid flowing and entropy production against vertical plate utilizing fractional derivative techniques. Kumar et al. [16] evaluated the use of optimal Homotopy Asymptotic Technique for nanoliquid transportation across Darcy Forchheimer field to the stagnation area via comparing spreading and stretching forces. Nguyen et al. [17] investigated the consequences of magnetic field application on the heat transport and entropy production of nanofluid via a microchannel including a triangle polystyrene wall.

Activation energy model is the minimal energy supplies required to conduct a chemical process. The kinetic energy of gases is the basis of such models. Such models are utilized in manufacturing and science issues. Oil emulsifiers, water mechanisms and food processing play important roles in the chemical industry and, owing to concentration of fluid there is a variation in the mixture-type mass transmission process. Geothermal sources have been investigated for exothermic and endothermic processes with the help of Arrhenius activation energy. Arrhenius activation energy can be expressed by Ea. The analysis of boundary layers including binary chemical processes was invented by Bestman [18]. He observed the movement of heat/mass transport throughout a porous medium with both the influence of binary reaction and activation energy. Abdelmalek et al. [19] assessed the gyrotactic motile organisms of nanomaterials in the distribution of modified micropolar liquid to the accelerated extended sheet. Transformation of the production of entropy in the radiation chemically viscous dissipation flowing of Prandtl–Eyring nanoliquid including Arrhenius activation energy is explored by Kanwal et al. [20]. Salahuddin et al. [21] summarized the steady-state velocity heat and mass transformation of the Casson nanofluid flow in the existence of a pre-exponential component across the vertical stretched pin. Ijaz et al. [22] reported the concerns with configuration of entropy production and the Arrhenius activation energy process for the nonlinear convectional flow of Sisko nanoliquid owing to the expandable revolving disk.

Developing variations in the absorption of micro-organisms induces, for example, bioconvection of algae as well as bacteria. Motion is a mechanism for the shared swimming bioconvective of bacteria. The characteristics of fluids may be influenced by self-directed microorganisms in the geometry presented. Due to the various applications of motile microorganisms in a variety of fields including ethanol, bio fertilizers and bio-fuels, investigators have begun their research in the area of motile microorganisms in a variety of fluid dynamic circumstances. Specific nanoparticles coupled with various free species, including

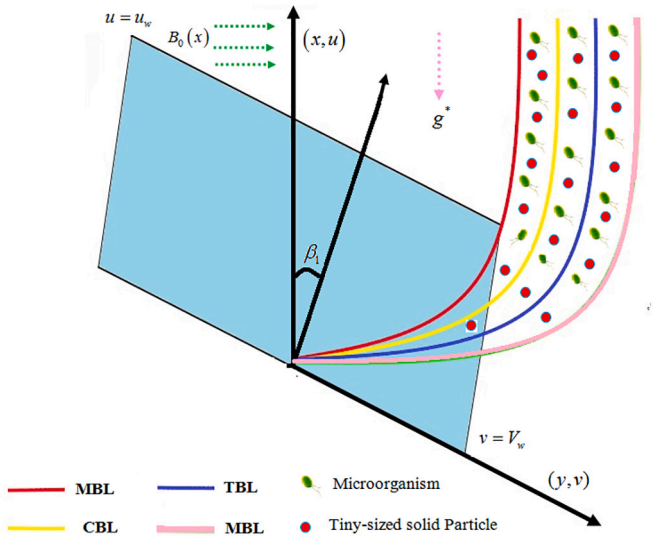

Fig. 1. Physical view of flow problem with coordinate system.

ciliates as well as flagellates, will improved situation efficiencies. Bioconvection has frequently the subject of discussion in numerous biotechnological fields, including on the fluids and their physiochemical characteristics. Platt [23] was firstly proposed the expression/word of bioconvection and identified rotating polygonal configurations in heavy Tetrahymena societies. Kuznetsov [24] introduced the observations of water-based combined nanoliquid application to oxyntic microorganisms. Eswaramoorthi et al. [25] investigated the Magnetohydrodynamic bioconvectional flow of heat Radiative nano fluid in a stratification medium through gyrotactic motile microorganisms. Nayak et al. [26] scrutinized the momentum, thermal, nanoparticles concentration and gyrotactic micro-organism (GM) slipping impacts on the chemically reactive Casson fluid flow under an exponentially extended magnetic surface in the existence of chemical reactions. The Bioconvection stagnation-point flowing of nanofluid including gyrotactic motile microorganisms over a nonlinear extending surface contained in a porous medium is mentioned by Mondal et al. [27]. Chamkha et al. [28] addressed the numerical simulation accentuates a combined bioconvectional flow over a vertical wedge throughout a Darcy permeable material filled by nanofluid including both nano-materials and gyrotactic motile microorganisms. Sajid et al. [29] studied the Double-diffuse tangent hyperbolic nanoliquid consisting motile microorganisms as well as Magnetohydrodynamic through a stretched surface. Ardekani et al. [30] examined the Soret and Dufour impact on a continuous mixed convection boundary layer movement over a vertical sheet in an electromagnetic field enclosed in a porous channel with gyrotactic motile microorganisms. Marin et al. [31] identified a mathematical analysis on the swim of migration patterns gyrotactic motile microorganisms in non-Newtonian blood-based nanoliquid through anisotropic narrowing arteries. Eldabe et al. [32] investigated the simultaneous radiation impacts, magnetization field and chemicals reactions on the peristaltic transport of non-Newtonian fluids including gyrotactic motile microorganisms and nano-materials. Hussain et al. [33] discussed the influences of Stefan blowing on the properties of heat and mass flux and the bioconvectional of self-motivated microbes combined in water-based nanoparticles with absorption of the leading

edge. Some investigators worked on gyrotactic microorganisms with bio-convective phenomenon containing different applications in various filed through ref.'s [34–39]. Oyelakin et al. [40] introduced the 2-D viscous boundary layer of mixed convective flowing heat and mass transformation against a vertical plate covered by Casson fluid embedded in a transparent quiescent medium including both nano-materials and gyrotactic motile microorganisms.

Current investigation presents the bio-convective nanofluid model for Brinkman type micropolar non-Newtonian fluid along with distinct thermal features confined by a stretched surface. The current model is subject to following novel features:

- The bioconvection aspects of Brinkman type micropolar nanofluid is examined in presence of magnetic applied magnetic force.
- The thermal properties of nanofluids are examined by utilizing temperature dependent heat source/sink and exponential space-based thermal source.
- In thermally developed flow, the nonlinear thermal radiation expressions are followed.
- The activation energy and melting heat transfer applications are also carried out.
- Further, concentration of nano-materials and thermal fields are considered in the occurrence of Brownian motion and thermophoresis diffusion.
- The numerical technique namely shooting method is developed to perform numerical computations.

2. Physical and mathematical modeling analysis

2.1. Physical description

The Robin boundary layer flow of Brinkman micropolar bio-convection nanofluid involving swimming microorganisms with melting process through a nonlinear stretching inclined surface is demonstrated. The energy and concentration equations are modeled with the performance of temperature dependent heat source/sink, exponential space-based thermal source and Arrhenius activation energy. The surface is stretched with free stream velocity $u_w(x) = ax$. The performance of Brownian and thermophoresis diffusions are analyzed for nanofluid. The components of velocity u and v are along the x-axis and $y-axis$ directions. The schematic physical view and coordinate system is described in Fig. 1.

2.2. Mathematical modeling

The following expressions of continuity, momentum, energy, concentration and microorganisms are formulated by adopting the above discussed physical descriptions:

$$\frac{\partial v}{\partial y} + \frac{\partial u}{\partial x} = 0, \tag{1}$$

$$u\frac{\partial u}{\partial x} + v\frac{\partial u}{\partial y} = \left(\frac{\mu + K_1^*}{\delta_f} + \mu(T)\right)\frac{\partial}{\partial y}\left(\frac{\partial u}{\partial y}\right) + \frac{K_1^*}{\delta_f}\frac{\partial N^*}{\partial y} - \left(\frac{\sigma^* B_0^2(x)}{\delta_f} - \beta^*\right)u + \frac{g^*}{\delta_f}\begin{bmatrix}(1-C_f)\delta_f\beta^{**}(T-T_\infty)\\ -(\delta_p-\delta_f)(C-C_\infty)\\ -(n-n_\infty)\gamma^{**}(\delta_m-\delta_f)\end{bmatrix}Cos\beta_1, \tag{2}$$

$$\delta j^*\left(u\frac{\partial N^*}{\partial x} + v\frac{\partial N^*}{\partial y}\right) = \frac{\partial}{\partial y}\left(\gamma^*\frac{\partial N^*}{\partial y}\right) - K_1^*\left(2N^* + \frac{\partial u}{\partial y}\right), \tag{3}$$

$$v\frac{\partial T}{\partial y} + u\frac{\partial T}{\partial x} = \left(\alpha_m + \frac{16\sigma^{**}T_\infty^3}{3(\delta c)_f k^*}\right)\frac{\partial^2 \widehat{T}}{\partial y^2} + \Gamma\left(D_B\left(\frac{\partial C}{\partial y}\frac{\partial T}{\partial y}\right) + \frac{D_T}{T_\infty}\left(\frac{\partial T}{\partial y}\right)^2\right) + \frac{Q}{(\delta c)_f}(T-T_\infty)$$
$$+\frac{Q^*}{(\delta c)_f}(T_w - T_\infty)exp\Big(-(a/\nu)^{0.5}ny\Big), \tag{4}$$

$$v\frac{\partial C}{\partial y} + u\frac{\partial C}{\partial x} + Kr^2(C-C_\infty)\left(\frac{T}{T_\infty}\right)^m exp\left(\frac{-E_a}{kT}\right) = D_B\frac{\partial^2 C}{\partial y^2} + \frac{D_T}{T_\infty}\frac{\partial^2 T}{\partial y^2}, \tag{5}$$

$$v\frac{\partial n}{\partial y} + u\frac{\partial n}{\partial y} = D_m\frac{\partial}{\partial y}\left(\frac{\partial n}{\partial y}\right) - \left[\frac{\partial}{\partial y}\left(n\frac{\partial C}{\partial y}\right)\right]\frac{bW_c}{\Delta C}, \tag{6}$$

with boundary conditions

$$u = u_w, v = V_w,\ N^* = -m_0^*\frac{\partial u}{\partial y}, -k\frac{\partial T}{\partial y} = h_f(T_w - T),$$
$$-D_B\frac{\partial C}{\partial y} = h_g(C_w - C), -D_m\frac{\partial n}{\partial y} = h_m(n_w - n), \quad \text{at } y = 0, \tag{7}$$

$$u \to u_\infty(x) = 0,\quad N^* \to 0, T \to T_\infty, C \to C_\infty, n \to n_\infty \ at\ y \to \infty. \tag{8}$$

Here μ indicates the viscosity, the magnetic field strength is B_0, σ^* designates the electric conductivity of fluid, N^* denotes the micro-rotation vector, β^* signifies Brinkman parameter coefficient, δ_f examines the fluid density, δ_p is the nanoparticles density, δ_m illustrates the

density of microorganisms, g^* is the acceleration due to gravity, $K_1{}^*$ is the material constant, β^* be a sign of volume exception coefficient, σ^{**} is Stefan-Boltzmann coefficient, k^* mean absorption coefficient, T for temperature, C for concentration, n the microorganisms, D_B Brownian motion coefficient, the coefficient of thermophoresis dispersion is denoted by D_T, Γ stands for the ratio between heat capacities, heat capacity of base fluid is symbolized by $(\delta c)_f$, Kr^2 symbolizes the chemical reaction constant, fitted rate constant is denoted by m, the activation energy coefficient isE_a, coefficient of microorganisms is denoted as D_m, b designates the chemotaxis constant and cell swimming speed is W_c.

The temperature base viscosity and melting boundary condition are given by

$$\mu(\theta) = e^{-(\gamma\theta)} = 1 - (\gamma\theta) + O(\gamma^2),$$
$$-k\left(\frac{\partial T}{\partial y}\right)\Big|_{y=0} = \delta[\lambda + (T_m - T_0)c_s] \tag{9}$$

2.3. Dimensionless formulation

Inspiring the following similarity transformation, system of boundary layer flow is reduced to a dimensionless system of ordinary ones.

$$u = axf'(\zeta), v = -\sqrt{a\nu}f(\zeta), \zeta = \sqrt{\frac{a}{\nu}}y,\ \ N^* = \sqrt{\frac{a}{\nu}}axg(\zeta),$$
$$\theta(\zeta) = \frac{T - T_\infty}{\Delta T},\ \ \phi(\zeta) = \frac{C - C_\infty}{\Delta C},\ \ \chi(\zeta) = \frac{n - n_\infty}{\Delta n}. \tag{10}$$

Introducing eq. (10) into expressions (1–6), continuity is automatically verified, eqs. (2–6) are simplify to

$$(1 + \Omega - (\gamma\theta))\frac{d^3f}{d\zeta^3} + (f - \gamma\theta')\frac{d^2f}{d\zeta^2} - \left(\frac{df}{d\zeta}\right)^2 + \Omega\frac{dg}{d\zeta} - (M - \beta)\frac{df}{d\zeta} + \alpha(\theta - Rb\phi - Rc\chi)cos\beta_1 = 0, \tag{11}$$

$$\left(1 + \frac{\Omega}{2}\right)\frac{d^2g}{d\zeta^2} + f\frac{dg}{d\zeta} - \frac{df}{d\zeta}g - \Omega\left(2g + \frac{d^2f}{d\zeta^2}\right) = 0, \tag{12}$$

$$\left(1 + \frac{4}{3}Rd\right)\frac{d^2\theta}{d\zeta^2} + PrNt\left(\frac{d\theta}{d\zeta}\right)^2 + Prf\frac{d\theta}{d\zeta} + PrNb\frac{d\theta}{d\zeta}\frac{d\phi}{d\zeta} + Q_E\theta + Q_Pexp(-n\zeta) + \frac{4}{3}Rd\left\{3(\theta_f - 1)\left[\theta\frac{d^2\theta}{d\zeta^2} + \left(\frac{d\theta}{d\zeta}\right)^2\right] + 3(\theta_f - 1)^2\left[2\theta\left(\frac{d\theta}{d\zeta}\right)^2 + \theta^2\frac{d^2\theta}{d\zeta^2}\right]\right\}$$
$$(\theta_f - 1)^3\left[3\theta^2\left(\frac{d\theta}{d\zeta}\right)^2 + \theta^3\frac{d^2\theta}{d\zeta^2}\right] = 0, \tag{13}$$

$$\frac{d^2\phi}{d\zeta^2} + \frac{Nt}{Nb}\left(\frac{d^2\theta}{d\zeta^2}\right) + LePr\left(f\frac{d\phi}{d\zeta}\right) - LePr\gamma^{\hat{}}(1 + \varpi\theta)^m\phi exp\left(-\frac{E}{1 + \varpi\theta}\right) = 0, \tag{14}$$

$$\frac{d^2\chi}{d\zeta^2} + Lbf\frac{d\chi}{d\zeta} - Pe\left(\frac{d^2\phi}{d\zeta^2}(\chi + \omega) + \frac{d\chi}{d\zeta}\frac{d\phi}{d\zeta}\right) = 0. \tag{15}$$

with

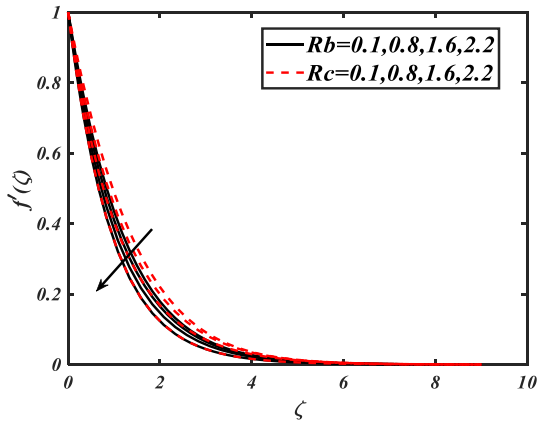

Fig. 2. Variation of Rb and Rc against $f'(\zeta)$.

$$Me\theta + Prf = 0, \frac{df}{d\zeta}(\zeta) = 1, g(\zeta) = -m_0^*f''(0), \frac{d\theta}{d\zeta} = -D_1(1 - \theta(\zeta)),$$
$$\frac{d\phi}{d\zeta} = -D_2(1 - \phi(\zeta)), \frac{d\chi}{d\zeta} = -D_3(1 - \chi(\zeta)) \quad at\ \zeta = 0, \tag{16}$$

$$f'(\zeta)\to 0, h(\zeta)\to 0, \theta(\zeta)\to 0, \phi(\zeta)\to 0, \chi(\zeta)\to 0, \ \ as\ \zeta\to\infty. \tag{17}$$

Here, magnetic parameter is $M = \frac{\sigma^* B_0^2(x)}{a\delta_f}$, $Me = \frac{c_p(T_\infty - T_m)}{\lambda + c_s(T_m - T_0)}$ indicates melting parameter, $\Omega = \frac{K_1^*}{\mu}$ indicates angular micropolar parameter, $\beta = \frac{\beta^*}{a}$ designates the Brinkman parameter, mixed convection parameter symbolized as $\alpha = \frac{a(1 - C_\infty)g^*\Delta T\beta^{**}}{\nu}$, $Rb = \frac{\Delta T(\delta_p - \delta_f)}{\beta^{**}\delta_f(1 - C_f)T_\infty}$ designates buoyancy ratio parameter, $Rc = \frac{\gamma^{**}(\delta_m - \delta_f)\Delta n}{\beta^{**}(1 - C_f)T_\infty}$denotes bioconvection Rayleigh number, Prandtl number represented by $Pr = \frac{\nu}{\alpha_m}$, $Nb = \ = \frac{D_B\Gamma\Delta C}{\nu}$specifies Brownian motion parameter, thermal-dependent heat source/sink parameter is captured as $Q_E = \frac{Q}{(\delta c)_f a}$, $Nt = \frac{D_T\Gamma\Delta T}{T_\infty\nu}$denotes thermophoresis parameter, $Q_P = \frac{Q^*}{(\delta c)_f a}$ specify the exponential space-dependent heat source parameter, temperature ratio parameter is$\theta_f = \frac{T_w}{T_\infty}$, temperature difference parameter is$\varpi = \frac{\Delta T}{T_\infty}$, Lewis number is read as$Le = \alpha/D_B$, $\gamma^{\hat{}} = \frac{Kr^2}{c}$ indicates the chemical reaction parameter, $E = \frac{E_a}{kT_\infty}$ dedicates the activation energy parameter, thermal radiation parameter is $Rd = \frac{4\sigma^{**}T_\infty^3}{k^*k}$, microorganism difference parameter is $\omega = \frac{n_\infty}{\Delta n}$, $Pe = \frac{bW_c}{D_m}$ signifies the Peclet number, $Lb = \frac{\nu}{D_m}$ indicates the bioconvection Lewis number, thermal Biot number is $D_1\left(= \frac{h_f}{k}\sqrt{\frac{\nu}{a}}\right)$, $D_2\left(= \frac{h_g}{D_B}\sqrt{\frac{\nu}{a}}\right)$ denotes mass Biot number and $D_3\left(= \frac{h_m}{D_m}\sqrt{\frac{\nu}{a}}\right)$symbolizes microorganisms Biot number.

2.4. Engineering interest

The industrial quantities of interest are:

$$Nu_x = \frac{xq_w}{k\Delta T}, Sh_x = \frac{xq_m}{D_B\Delta C}, Sn_x = \frac{xq_n}{D_m\Delta n}, \tag{18}$$

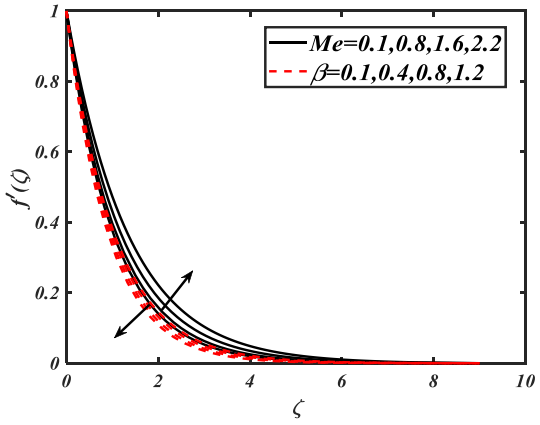

Fig. 3. Variation of Me and β against $f'(\zeta)$.

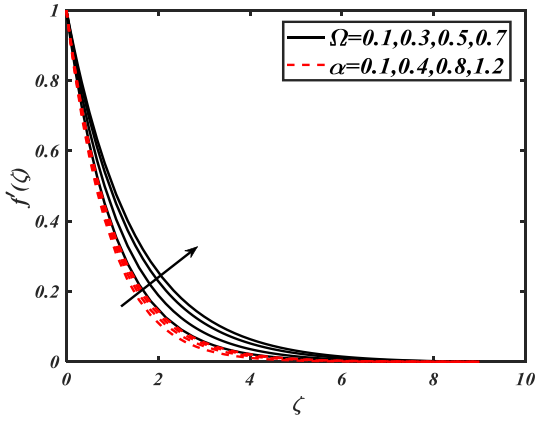

Fig. 4. Variation of Ω and α against $f'(\zeta)$.

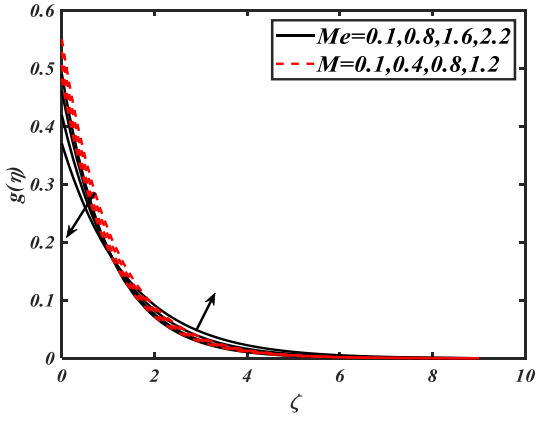

Fig. 5. Variation of Me and M against $g(\zeta)$.

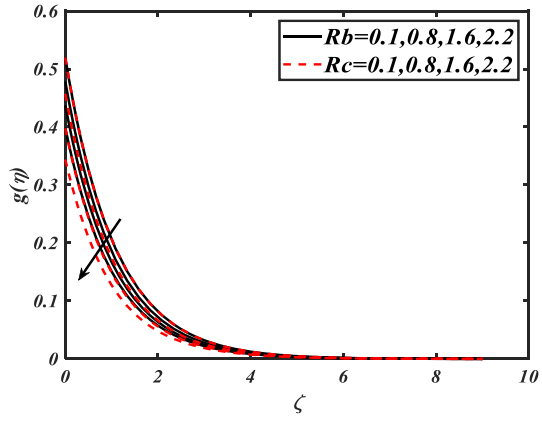

Fig. 6. Variation of Rb and Rc against $g(\zeta)$.

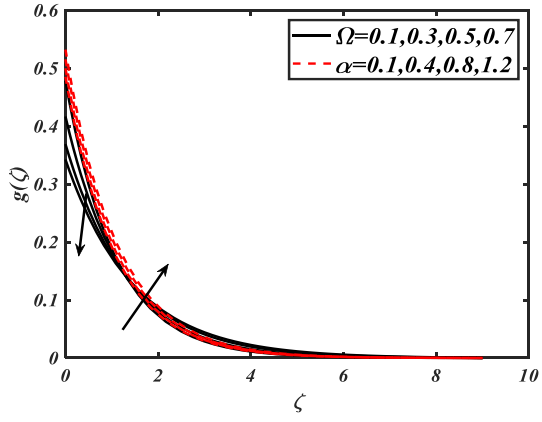

Fig. 7. Variation of Ω and α against $g(\zeta)$.

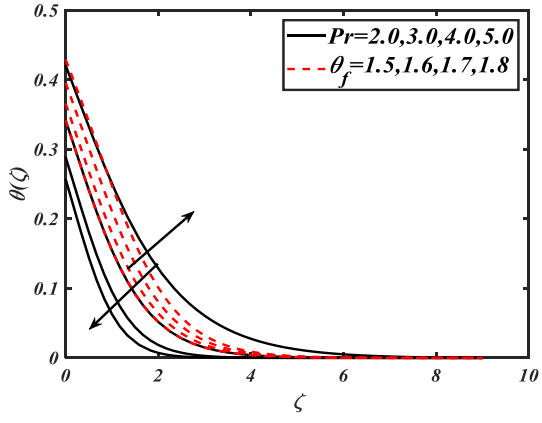

Fig. 8. Variation of Pr and θ_f against $\theta(\zeta)$.

The dimensionless physical quantities are:

$$-\frac{d\theta(0)}{d\zeta}=\frac{Nu_x}{\left(1+\frac{4}{3}Rd\right)\sqrt{Re_x}},\ -\frac{d\phi(0)}{d\zeta}=\frac{Sh_x(0)}{\sqrt{Re_x}},\ -\frac{d\phi(0)}{d\zeta}=\frac{Sn_x(0)}{\sqrt{Re_x}}. \tag{19}$$

Here $Re_x=\frac{u_w x}{\nu}$ designates the local Reynolds number.

3. Numerical method

In this section, the Magnetohydrodynamic boundaries layer flow of micropolar nanofluid with slipping is introduced. Specification of the numerical technique utilized was carried out in specific cases of the method and the findings produced were associated with the current solutions in the scientific literature. Provides a numerically solution for non-dimensional nonlinear velocities, temperatures, nanoparticles concentrations and gyrotactic motile microorganisms equations. In nature

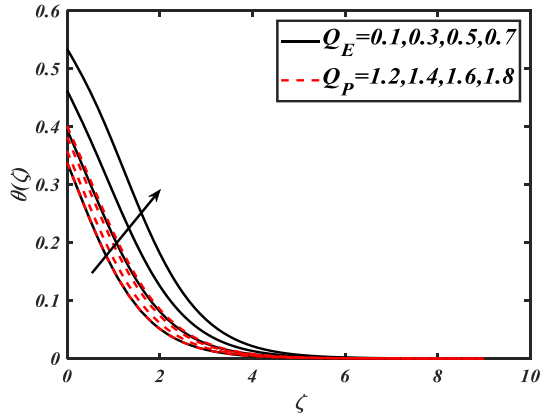

Fig. 9. Variation of Q_E and Q_E against $\theta(\zeta)$.

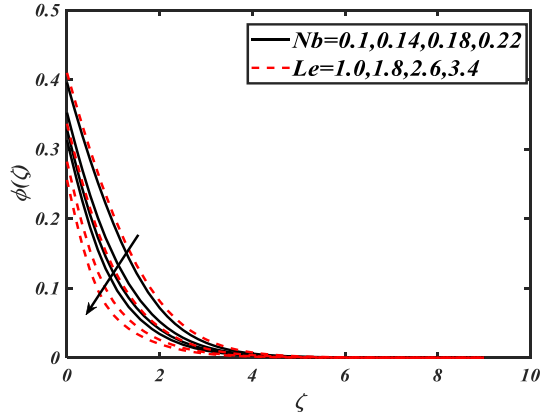

Fig. 10. Variation of *Nb* and *Le* against $\phi(\zeta)$.

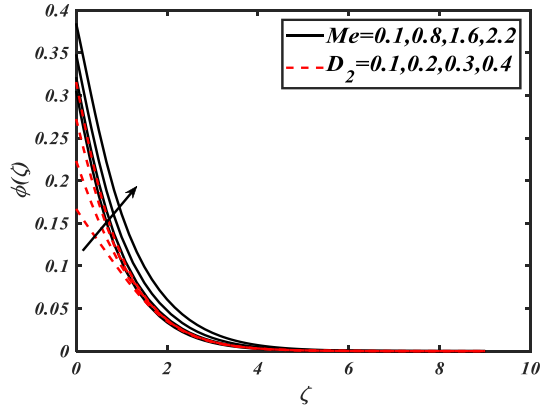

Fig. 11. Variation of *Me* and D_2 against $\phi(\zeta)$.

the governing partial differential equations and slipping boundary constraints are strongly non-linear. The method of fundamental dimensionless governing of steady and unsteady combined equations is distinguished numerically by implementing the shooting scheme. Here the numerically solutions for specified Eqs. (11–15). Such equations are numerically solved along with accompanied boundary constraints (16–17) by a proficient algorithm of computational MATLAB shooting scheme bvp4c for various physical model parameters. In order to apply this technique, we must first convert into a system of first-order equations with the description of innovative variables.

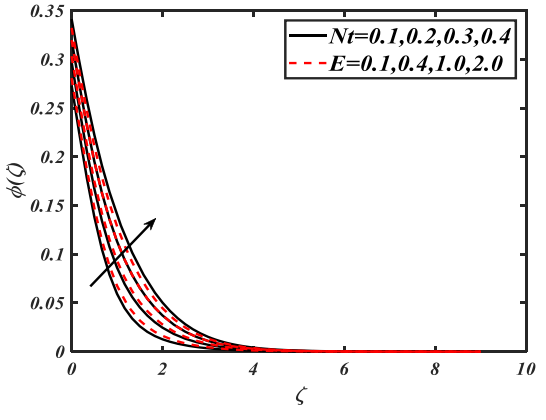

Fig. 12. Variation of *Nt* and *E* against $\phi(\zeta)$.

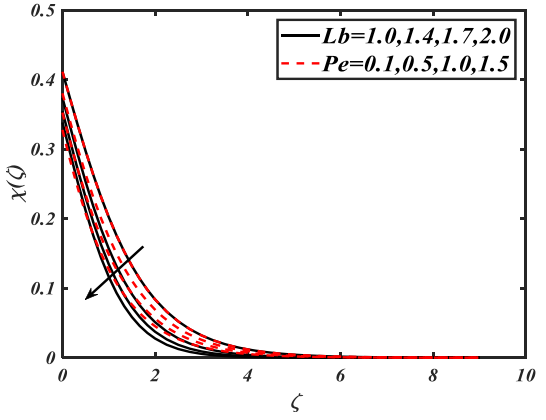

Fig. 13. Variation of *Lb* and *Pe* against $\chi(\zeta)$.

$$f = q_1, \frac{df}{d\zeta} = q_2, \frac{d^2f}{d\zeta^2} = q_3, \frac{d^3f}{d\zeta^3} = q_3^{'},$$

$$g = q_4, \frac{dg}{d\zeta} = q_5, \frac{d^2g}{d\zeta^2} = q_5^{'}, \theta = q_6,$$

$$\frac{d\theta}{d\zeta} = q_7, \frac{d^2\theta}{d\zeta^2} = q_7^{'}, \phi = q_8, \frac{d\phi}{d\zeta} = q_9, \tag{20}$$

$$\frac{d^2\phi}{d\zeta^2} = q_9^{'}, \chi = q_{10}, \frac{d\chi}{d\zeta} = q_{11}, \frac{d^2\chi}{d\zeta^2} = q_{11}^{'},$$

$$q_3^{'} = \frac{-(q_1 - \gamma q_7)q_3 + (q_2)^2 - \Omega q_5 + (M - \beta)q_2 - \alpha(q_6 - Rbq_8 - Rcq_{10})cos\beta_1}{(1 + \Omega - (\gamma q_6))}, \tag{21}$$

$$q_5^{'} = \frac{-q_1 q_5 + q_2 q_4 + \Omega(2q_4 + q_3)}{\left(1 + \frac{\Omega}{2}\right)}, \tag{22}$$

$$q_7^{'} = \frac{-PrNbq_7q_9 - Q_E q_6 - Q_P exp(-n\zeta) - PrNtq_7^2 - Prfq_7 - \frac{4}{3}Rd\left\{3(\theta_f - 1)[+(q_7)^2] + 3(\theta_f - 1)^2[2q_6q_7^2] + 3(\theta_f - 1)^3[3q_6^2q_7^2]\right\}}{\left(1 + \frac{4}{3}Rd\right) + \frac{4}{3}Rd\left[3(\theta_f - 1)q_6 + 3(\theta_f - 1)^2q_6^2 + 3(\theta_f - 1)^3q_6^3\right]}, \tag{23}$$

$$q_9^{'} = -\frac{Nt}{Nb}(q_7^{'}) - LePr(q_1q_9) + LePr\hat{\gamma}(1 + \varpi q_6)^m q_8 exp\left(-\frac{E}{1 + \varpi q_6}\right), \tag{24}$$

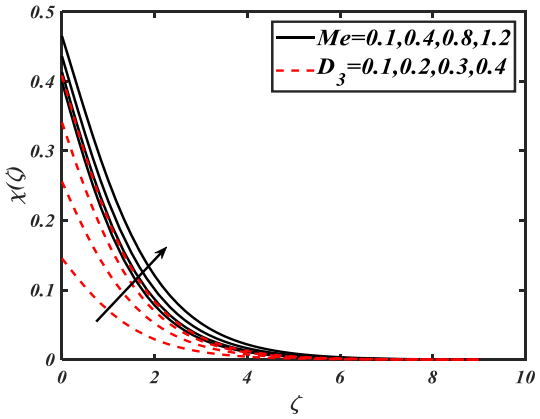

Fig. 14. Variation of *Me* and D_3 against $\chi(\zeta)$.

$$q_{11}^{'} = -Lbq_1q_{11} + Pe\left(q_9^{'}(\chi+\omega) + q_{11}q_9\right) \tag{25}$$

with

$$\begin{aligned} &Meq_6 + Prq_1 = 0, q_2(\zeta) = 1, q_4(\zeta) = -m_0^{*}q_3, q_7 = -D_1(1-q_6(\zeta)), \\ &q_9 = -D_2(1-q_8(\zeta)), q_{11} = -D_3(1-q_{10}(\zeta)) \quad at\ \zeta = 0, \end{aligned} \tag{26}$$

$$f^{'}(\zeta)\to 0, h(\zeta)\to 0, \theta(\zeta)\to 0, \phi(\zeta)\to 0, \chi(\zeta)\to 0, \quad as\ \zeta\to\infty. \tag{27}$$

4. Result and discussion

The results with physical relevance against various flow parameters are explained by sketching various graphs. Each physical parameter get varied with some specified numerical values to observe the change in velocity, temperature, concentration and microorganisms distributions. Fig. 2 is devoted to scrutinize the simultaneous performance of buoyancy ratio parameter *Rb* and bioconvection Rayleigh number *Rc* on velocity field$f'(\zeta)$. It is obvious that the increase in buoyancy ratio parameter *Rb* and bioconvection Rayleigh number *Rc* depresses the velocity field$f'(\zeta)$. To illustrate the impact of melting parameter *Me* and Brinkman parameter β on velocity field $f'(\zeta)$ Fig. 3 is captured. Our computation depict that enlarge in melting parameter *Me* rise the velocity field$f'(\zeta)$. From this analysis it is noted that velocity field $f'(\zeta)$ is retarded by growing the values of Brinkman parameter β. Micro-rotation material parameter Ω and mixed convection parameter α on velocity field $f'(\zeta)$ are indicated in Fig. 4. A rise in velocity $f'(\zeta)$ curves with larger Micro-rotation material parameter Ω and mixed convection parameter α is investigated. The impacts of magnetic parameter *M* and melting parameter *Me* on angular velocity $g(\zeta)$ are plotted in Fig. 5, it can be scrutinized that angular velocity $g(\zeta)$ reduces for greater magnetic parameter *M* while raised with melting parameter *Me*. It is in accordance with the physical expectation for which magnetic field creates a resistive force that acts in the opposite direction of the fluid. Fig. 6 represents the trend of angular velocity $g(\zeta)$ for enhancing values buoyancy ratio parameter *Rb* and bioconvection Rayleigh number *Rc*. It is witnessed that angular velocity $g(\zeta)$ is an increasing function of both parameters. In order to illustrate the impact of micro-rotation material parameter Ω and mixed convection parameter α on angular velocity$g(\zeta)$, Fig. 7 is tired. The performance of angular velocity $g(\zeta)$ is decline near the boundary layer surface while rises away from the surface for higher variations of micro-rotation material parameter Ω. A growing estimation of mixed convection parameter α result an increasing angular velocity $g(\zeta)$ of fluid.

The interpretation of Prandtl number *Pr* and temperature ratio parameter θ_f on thermal field of species $\theta(\zeta)$ is reported in Fig. 8. Temperature distribution $\theta(\zeta)$ illustrated decreasing behavior for larger values of Prandtl number *Pr*, while opposite trend for temperature ratio parameter θ_f is noted. Fig. 9 is designed to estimate the behavior of temperature dependent heat source/sink Q_E and exponential space-base heat source parameter Q_P. An increment in temperature field $\theta(\zeta)$ is observed, as we enhance the values of temperature dependent heat source/sink Q_E and exponential space-base heat source parameter Q_P.

The effect of Brownian motion parameter *Nb* and Lewis number *Le* on volumetric concentration of nanoparticles $\phi(\zeta)$ is complied in Fig. 10. Performance of concentration fields $\phi(\zeta)$ shows reducing trend for higher Brownian motion parameter *Nb* and Lewis number *Le*. Fig. 11 is

Table 1
Numerical values of local Skin friction coefficient $-f''(0)$ for different magnitudes of substantial parameters.

β	Ω	*M*	α	*Rb*	*Rc*	*Me*	$-f''(0)$
0.2	0.1	0.1	0.1	0.1	0.1	0.3	0.9600
0.4							0.7935
0.8							0.5757
0.1	0.2	0.1	0.1	0.1	0.1	0.3	0.9283
							0.8900
	0.4						0.8259
	0.8						
0.1	0.1	0.2	0.1	0.1	0.1	0.3	0.9958
		0.6					1.1617
		1.0					1.3059
0.1	0.1	0.1	0.2	0.1	0.1	0.3	0.8850
			0.4				0.8460
			0.8				0.7735
0.1	0.1	0.1	0.1	0.2	0.1	0.3	0.9077
							0.9253
				1.0			0.9481
				2.0			
0.1	0.1	0.1	0.1	0.1	0.2	0.3	0.9078
					1.0		0.9259
					2.0		0.9494
0.1	0.1	0.1	0.1	0.1	0.1	0.5	0.8699
						1.0	0.7692
						1.5	0.6432

Table 2
Numerical values of local microrotation coefficient $-g'(0)$ for different magnitudes of substantial parameters.

β	Ω	*M*	α	*Rb*	*Rc*	*Me*	$-g'(0)$
0.2	0.1	0.1	0.1	0.1	0.1	0.3	0.4187
0.4							0.3765
0.8							0.2769
0.1	0.2	0.1	0.1	0.1	0.1	0.3	0.4191
							0.3868
	0.4						0.3347
	0.8						
0.1	0.1	0.2	0.1	0.1	0.1	0.3	0.4543
		0.6					0.5127
		1.0					0.5600
0.1	0.1	0.1	0.2	0.1	0.1	0.3	0.4144
			0.4				0.3993
			0.8				0.3695
0.1	0.1	0.1	0.1	0.2	0.1	0.3	0.4228
							0.4293
				1.0			0.4375
				2.0			
0.1	0.1	0.1	0.1	0.1	0.2	0.3	0.4228
							0.4297
					1.0		0.4384
					2.0		
0.1	0.1	0.1	0.1	0.1	0.1	0.5	0.3904
						1.0	0.3080
						1.5	0.2186

Table 3
Numerical values of local Nusselt number $-\theta'(0)$ for different magnitudes of substantial parameters.

β	Ω	M	α	Rb	Rc	Me	Pr	Nb	Nt	Rd	D_1	$-\theta'(0)$
0.2	0.1	0.1	0.1	0.1	0.1	0.3	1.2	0.2	0.3	0.5	0.3	0.1740
0.4												0.1781
0.8												0.1834
0.1	0.2	0.1	0.1	0.1	0.1	0.3	1.2	0.2	0.3	0.5	0.3	0.1728
	0.4											0.1744
	0.8											0.1769
0.1	0.1	0.2	0.1	0.1	0.1	0.3	1.2	0.2	0.3	0.5	0.3	0.1700
		0.6										0.1629
		1.0										0.1566
0.1	0.1	0.1	0.2	0.1	0.1	0.3	1.2	0.2	0.3	0.5	0.3	0.1752
			0.4									0.1768
			0.8									0.1793
0.1	0.1	0.1	0.1	0.2	0.1	0.3	1.2	0.2	0.3	0.5	0.3	0.1742
				1.0								0.1733
				2.0								0.1723
0.1	0.1	0.1	0.1	0.1	0.2	0.3	1.2	0.2	0.3	0.5	0.3	0.1744
					1.0							0.1735
					2.0							0.1725
0.1	0.1	0.1	0.1	0.1	0.1	0.5	1.2	0.2	0.3	0.5	0.3	0.1682
						1.0						0.1474
						1.5						0.1125
0.1	0.1	0.1	0.1	0.1	0.1	0.3	1.5	0.2	0.3	0.5	0.3	0.1845
												0.1985
							2.0					0.2079
							2.5					
0.1	0.1	0.1	0.1	0.1	0.1	0.3	1.2	0.4	0.3	0.5	0.3	0.1689
												0.1628
								0.8				0.1565
								1.2				
0.1	0.1	0.1	0.1	0.1	0.1	0.3	1.2	0.2	0.4	0.5	0.3	0.1706
									0.8			0.1650
									1.2			0.1591
0.1	0.1	0.1	0.1	0.1	0.1	0.3	1.2	0.2	0.3	0.4	0.3	0.1766
										0.6		0.1543
										0.8		0.1322
0.1	0.1	0.1	0.1	0.1	0.1	0.3	1.2	0.2	0.3	0.5	0.5	0.2213
											1.0	0.2726
											1.5	0.2938

captured to study the impact of mass Biot number D_2 and melting parameter Me against concentration field $\phi(\zeta)$. We analyzed that concentration field $\phi(\zeta)$ rises when mass Biot number D_2 and melting parameter Me are boosted. The performance of thermophoresis parameter Nt and Activation energy parameter E versus concentration of nanoparticles $\phi(\zeta)$ is studied through Fig. 12. Here concentration of nanoparticles $\phi(\zeta)$ boosted up by increasing the values of thermophoresis parameter Nt and activation energy parameter E.

Fig. 13 reveals that microorganism's field $\chi(\zeta)$ diminishes for larger values of Peclet number Pe and bioconvection Lewis number Lb. In order to observe the trend of microorganism's $\chi(\zeta)$ curves for distinguish values of melting parameter Me and microorganisms Biot number D_3, Fig. 14 is sketched. From these curves it is depicted that concentration of microorganism $\chi(\zeta)$ augmented with greater amount of melting parameter Me and microorganisms Biot number D_3.

The numerical outcomes of local skin friction coefficient$-f''(0)$, local microrotation coefficient$-g'(0)$, local Nusselt number$-\theta'(0)$, local Sherwood number$-\phi'(0)$ and local microorganism density number $-\chi'(0)$ are examined and elaborated through Tables 1–5. From Tables 1–2, it can be examined that the skin friction coefficient $-f''(0)$ and microrotation coefficient $-g'(0)$ are reduced for mixed convection parameter α and Brinkman parameter β while both are rise with bioconvection Rayleigh number Rc and buoyancy ratio parameter Rb. Form Tables 3–4 it is observed that the local Nusselt number $-\theta'(0)$ and local Sherwood number $-\phi'(0)$ are depressed by increasing thermophoresis parameter Ntr. Table 5 is drawn to examine the behavior of local microorganism's density number $-\chi'(0)$ against flow parameters. It is observed that a local microorganism density number $-\chi'(0)$ is diminishes for larger Melting parameter Me and microrotation parameter Ω while inverse behavior is analyzed for Peclet number Pe and bioconvection Lewis number Lb.

Table 4
Numerical values of local Sherwood number $-\phi'(0)$ for different magnitudes of substantial parameters.

β	Ω	M	α	Rb	Rc	Me	Pr	Nb	Nt	Le	D_2	$-\phi'(0)$
0.2	0.1	0.1	0.1	0.1	0.1	0.3	1.2	0.2	0.3	2.0	0.4	0.2390
												0.2439
0.4												0.2501
0.8												
0.1	0.2	0.1	0.1	0.1	0.1	0.3	1.2	0.2	0.3	2.0	0.4	0.2377
												0.2394
	0.4											0.2423
	0.8											
0.1	0.1	0.2	0.1	0.1	0.1	0.3	1.2	0.2	0.3	2.0	0.4	0.2344
		0.6										0.2262
		1.0										0.2189
0.1	0.1	0.1	0.2	0.1	0.1	0.3	1.2	0.2	0.3	2.0	0.4	0.2404
												0.2422
			0.4									0.2451
			0.8									
0.1	0.1	0.1	0.1	0.2	0.1	0.3	1.2	0.2	0.3	2.0	0.4	0.2392
				1.0								0.2383
				2.0								0.2371
0.1	0.1	0.1	0.1	0.1	0.2	0.3	1.2	0.2	0.3	2.0	0.4	0.2393
					1.0							0.2384
					2.0							0.2372
0.1	0.1	0.1	0.1	0.1	0.1	0.5	1.2	0.2	0.3	2.0	0.4	0.2300
						1.0						0.1964
						1.5						0.1350
0.1	0.1	0.1	0.1	0.1	0.1	0.3	1.5	0.2	0.3	2.0	0.4	0.2540
							2.0					0.2737
							2.5					0.2871
0.1	0.1	0.1	0.1	0.1	0.1	0.3	1.2	0.4	0.3	2.0	0.4	0.2550
												0.2636
								0.8				0.2659
								1.2				
0.1	0.1	0.1	0.1	0.1	0.1	0.3	1.2	0.2	0.4	2.0	0.4	0.2252
												0.1833
									0.8			0.1476
									1.2			
0.1	0.1	0.1	0.1	0.1	0.1	0.3	1.2	0.2	0.3	3.0	0.4	0.2641
										4.0		0.2803
										5.0		0.2913
0.1	0.1	0.1	0.1	0.1	0.1	0.3	1.2	0.2	0.3	2.0	0.5	0.2776
											1.0	0.4077
											1.5	0.4832

5. Concluding remarks

The bioconvection flow of Brinkman type micropolar fluid due to a stretching inclined surface are analyzed in presence of melting heat transfer. The exponential heat source, thermal radiation and activation energy relations are also imposed to modify the nanofluid analysis. To acquire the numerical results of the problem, bvp4c tool of MATLAB is implemented. The significant outcomes of current flow problem are given below:

- A retarded change in velocity is noticed with melting parameter and Hartmann number.
- An increasing change in velocity has been observed with angular micropolar parameter and mixed convection constant.
- The presence of buoyancy ratio parameter and melting parameter depressed the angular velocity.
- The nanofluid temperature improved with exponential space-dependent heat source parameter and heat source constant.
- The concentration of nanofluid is diminishes for Lewis number while improves with larger activation energy and melting parameter.
- Increasing values of mass Biot number and melting parameter cause an increment in concentration.
- An increasing behavior microorganism is noticed for a larger microorganisms Biot number.
- Larger bioconvection Lewis number and Peclet number decrease the concentration of microorganism.

Declaration of Competing Interest

The authors declare that they have no known competing financial interests or personal relationships that could have appeared to influence the work reported in this paper.

Table 5
Numerical values of local microorganism's density number $-\chi'(0)$ for different magnitudes of substantial parameters.

β	Ω	M	α	Rb	Rc	Me	Pe	Lb	D_3	$-\chi'(0)$
0.2	0.1	0.1	0.1	0.1	0.1	0.3	0.1	1.0	0.4	0.2313
0.4										0.2362
0.8										0.2426
0.1	0.2	0.1	0.1	0.1	0.1	0.3	0.1	1.0	0.4	0.2300
	0.4									0.2318
	0.8									0.2347
0.1	0.1	0.2	0.1	0.1	0.1	0.3	0.1	1.0	0.4	0.2267
		0.6								0.2183
		1.0								0.2107
0.1	0.1	0.1	0.2	0.1	0.1	0.3	0.1	1.0	0.4	0.2327
										0.2346
			0.4							0.2375
			0.8							
0.1	0.1	0.1	0.1	0.2	0.1	0.3	0.1	1.0	0.4	0.2315
										0.2306
				1.0						0.2294
				2.0						
0.1	0.1	0.1	0.1	0.1	0.2	0.3	0.1	1.0	0.4	0.2316
					1.0					
					2.0					0.2307
										0.2295
0.1	0.1	0.1	0.1	0.1	0.1	0.5	0.1	1.0	0.4	0.2228
						1.0				0.1924
						1.5				0.1391
0.1	0.1	0.1	0.1	0.1	0.1	0.3	0.4	1.0	0.4	0.2426
							0.8			0.2557
							1.2			0.2673
0.1	0.1	0.1	0.1	0.1	0.1	0.3	0.1	2.0	0.4	0.2681
								3.0		0.2858
								4.0		0.6968
0.1	0.1	0.1	0.1	0.1	0.1	0.3	0.1	1.0	0.5	0.2619
									1.0	0.3543
									1.5	0.4016

References

[1] S.U.S. Choi, Enhancing thermal conductivity of fluids with nanoparticles, Proc ASME Int. Mech. Eng. Congr. Exposition 66 (1995) 99–105.
[2] J. Buongiorno, Convective transport in nanofluids, J. Heat Transf. 128 (2006) 240–250.
[3] W. Ibrahim, M. Negera, Melting and viscous dissipation effect on upper-convected Maxwell and Williamson nanofluid, Eng. Rep. 5 (2) (2020), e12159.
[4] V.K. Sinha, B. Kumar, G.S. Seth, R. Nandkeolyar, Outlining the impact of thermal radiation on micropolar nanofluid viscous dissipative flow: A spectral method based numerical simulation with regression analysis, AIP Conf. Proc. 2253 (1) (2020, August) 020024. AIP Publishing LLC.
[5] A.V. Roşca, N.C. Roşca, I. Pop, Mixed convection stagnation point flow of a hybrid nanofluid past a vertical flat plate with a second order velocity model, Int. J. Num. Methods Heat & Fluid Flow. 31 (1) (2020) 75–91.
[6] Nayak, M. K., Saranya, S., Ganga, B., Hakeem, A. K. A., Sharma, R. P., & Makinde, O. D. Influence of relaxation-retardation viscous dissipation on chemically reactive flow of Oldroyd-B nanofluid with hyperbolic boundary conditions. Heat Transfer.
[7] F. Mabood, T.A. Yusuf, W.A. Khan, Cu–Al 2 O 3–H 2 O hybrid nanofluid flow with melting heat transfer, irreversibility analysis and nonlinear thermal radiation, J. Therm. Anal. Calorim. (2020) 1–12.
[8] A. Arjmandfard, D. Toghraie, B. Mehmandoust, M. Hashemian, A. Karimipour, The study of atomic porosity effect on water/Fe nanofluid flow in a microchannel with a molecular dynamics method, J. Mol. Liq. 317 (2020) 114291.
[9] K. Muhammad, T. Hayat, A. Alsaedi, B. Ahmad, Melting heat transfer in squeezing flow of basefluid (water), nanofluid (CNTs+ water) and hybrid nanofluid (CNTs+ CuO+ water), J. Therm. Anal. Calorim. (2020) 1–18.
[10] X. Cui, X. Cheng, H. Xu, B. Li, J. Zhu, Enhancement of thermophysical coefficients in nanofluids: a simulation study, Int. J. Mod. Phys. B 34 (25) (2020) 2050222.
[11] S. Marzougui, F. Mebarek-Oudina, A. Assia, M. Magherbi, Z. Shah, K. Ramesh, Entropy generation on magneto-convective flow of copper–water nanofluid in a cavity with chamfers, J. Therm. Anal. Calorim. (2020) 1–12.
[12] T. Muhammad, H. Waqas, S.A. Khan, R. Ellahi, S.M. Sait, Significance of nonlinear thermal radiation in 3D Eyring-Powell nanofluid flow with Arrhenius activation energy, J. Therm. Anal. Calorim. (2020) 1–16.
[13] H. Waqas, M. Imran, S.U. Khan, S.A. Shehzad, M.A. Meraj, Slip flow of Maxwell viscoelasticity-based micropolar nanoparticles with porous medium: a numerical study, Appl. Math. Mech. 40 (9) (2019) 1255–1268.
[14] U. Yashkun, K. Zaimi, N.A.A. Bakar, A. Ishak, I. Pop, MHD hybrid nanofluid flow over a permeable stretching/shrinking sheet with thermal radiation effect, Int. J. Num. Methods Heat & Fluid Flow. 31 (1) (2020) 1014–1031.
[15] S.E. Ahmed, A.A. Arafa, Impacts of the fractional derivatives on unsteady magnetohydrodynamics radiative Casson nanofluid flow combined with joule heating, Phys. Scr. 95 (9) (2020), 095206.
[16] R. Kumar, R. Kumar, T. Sharma, M. Sheikholeslami, Mathematical modeling of stagnation region nanofluid flow through Darcy–Forchheimer space taking into account inconsistent heat source/sink, J. Appl. Math. Comput. (2020) 1–22.
[17] Q. Nguyen, D. Bahrami, R. Kalbasi, Q.V. Bach, Nanofluid flow through microchannel with a triangular corrugated wall: heat transfer enhancement against entropy generation intensification, Math. Methods Appl. Sci. (2020), https://doi.org/10.1002/mma.6705.
[18] A.R. Bestman, Natural convection boundary layer with suction and masstransfer in a porous medium, Int. J. Energy Res. 14 (4) (1990) 389–396.
[19] Z. Abdelmalek, S.U. Khan, M. Awais, M.S. Mustfa, I. Tlili, Analysis of generalized micropolar nanofluid with swimming of microorganisms over an accelerated surface with activation energy, J. Therm. Anal. Calorim. (2020) 1–13.
[20] S. Qayyum, T. Hayat, M. Kanwal, A. Alsaedi, M.I. Khan, Transportation of entropy optimization in radiated chemically dissipative flow of Prandtl–Eyring nanofluid with activation energy, Comput. Methods Prog. Biomed. 184 (2020) 105130.
[21] T. Salahuddin, N. Siddique, M. Arshad, I. Tlili, Internal energy change and activation energy effects on Casson fluid, AIP Adv. 10 (2) (2020), 025009.
[22] M. Ijaz, M. Ayub, M.Y. Malik, H. Khan, A.A. Alderremy, S. Aly, Entropy analysis in nonlinearly convective flow of the Sisko model in the presence of joule heating and activation energy: the Buongiorno model, Phys. Scr. 95 (2) (2020), 025402.
[23] J.R. Platt, Bioconvection patterns in cultures of free-swimming organisms, Science 133 (80) (1961) 1766–1767.
[24] A.V. Kuznetsov, Nanofuid bioconvection in water-based suspensions containing nanoparticles and oxytactic microorganisms: oscillatory instability, Nanoscale Res. Lett. 6 (2011) 100.
[25] S. Eswaramoorthi, K. Jagan, S. Sivasankaran, MHD bioconvective flow of a thermally radiative nanoliquid in a stratified medium considering gyrotactic microorganisms, J. Phys. Conf. Ser. 1597 (1) (2020, July) 012001. IOP Publishing.
[26] M.K. Nayak, J. Prakash, D. Tripathi, V.S. Pandey, S. Shaw, O.D. Makinde, 3D bioconvective multiple slip flow of chemically reactive Casson nanofluid with gyrotactic microorganisms, Heat Transf. Asian Res. 49 (1) (2020) 135–153.
[27] S.K. Mondal, D. Pal, Mathematical analysis for Brownian motion of nonlinear thermal bioconvective stagnation point flow in a nanofluid using DTM and RKF method, J. Comput. Design Eng. 7 (3) (2020) 294–307.
[28] A.J. Chamkha, H.A. Nabwey, Z.M.A. Abdelrahman, A.M. Rashad, Mixed bioconvective flow over a wedge in porous media drenched with a Nanofluid, J. Nanofluids 9 (1) (2020) 24–35.
[29] T. Sajid, M. Sagheer, S. Hussain, F. Shahzad, Impact of double-diffusive convection and motile gyrotactic microorganisms on magnetohydrodynamics bioconvection tangent hyperbolic nanofluid, Open Phys. 18 (1) (2020) 74–88.

[30] N.I. Nima, M. Ferdows, M.M. Ardekani, Effects of cross diffusion and radiation on magneto mixed convective stagnation flow from a vertical surface in porous media with Gyrotactic microorganisms: similarity and numerical analysis, Spec. Top. Rev. Porous Media Int. J. 11 (3) (2020).
[31] M.M. Bhatti, M. Marin, A. Zeeshan, R. Ellahi, S.I. Abdelsalam, Swimming of motile Gyrotactic microorganisms and nanoparticles in blood flow through Anisotropically tapered arteries, Front. Phys. 8 (2020) 95.
[32] N.T. Eldabe, A.A. Zaghrout, S.F. Ramadan, H.A. Azzam, Simultaneous effects of radiation, magnetic field on peristaltic flow of Carreau nanofluid submerged in gyrotactic microorganisms with heat and mass transfer, Heat Transfer. 50 (2) (2020) 1198–1217.
[33] B. Ali, S. Hussain, S. Abdal, M.M. Mehdi, Impact of Stefan blowing on thermal radiation and Cattaneo–Christov characteristics for nanofluid flow containing microorganisms with ablation/accretion of leading edge: FEM approach, Eur. Phys. J. Plus 135 (10) (2020) 1–18.
[34] H. Waqas, M. Imran, T. Muhammad, S.M. Sait, R. Ellahi, Numerical investigation on bioconvection flow of Oldroyd-B nanofluid with nonlinear thermal radiation and motile microorganisms over rotating disk, J. Therm. Anal. Calorim. (2020), https://doi.org/10.1007/s10973-020-09728-2.
[35] S.U. Khan, H. Waqas, T. Muhammad, M. Imran, S. Aly, Simultaneous effects of bioconvection and velocity slip in three-dimensional flow of Eyring-Powell nanofluid with Arrhenius activation energy and binary chemical reaction, Int. Commun. Heat Mass Transf. 117 (2020) 104738.
[36] S.U. Khan, H. Waqas, T. Muhammad, M. Imran, M.Z. Ullah, Significance of activation energy and Wu's slip features in cross nanofluid with motile microorganisms, Commun. Theor. Phys. 72 (10) (2020) 105001.
[37] H. Waqas, S.A. Khan, S.U. Khan, M.I. Khan, S. Kadry, Y.M. Chu, Falkner-Skan time-dependent bioconvrction flow of cross nanofluid with nonlinear thermal radiation, activation energy and melting process, in: International Communications in Heat and Mass Transfer, 2020, p. 105028.
[38] H. Waqas, S.U. Khan, M. Imran, M.M. Bhatti, Thermally developed Falkner–Skan bioconvection flow of a magnetized nanofluid in the presence of a motile gyrotactic microorganism: Buongiorno's nanofluid model, Phys. Scr. 94 (11) (2019) 115304.
[39] H. Waqas, M. Imran, M.M. Bhatti, Influence of bioconvection on Maxwell nanofluid flow with the swimming of motile microorganisms over a vertical rotating cylinder, Chin. J. Phys. 68 (2020) 558–577.
[40] I.S. Oyelakin, S. Mondal, P. Sibanda, D. Sibanda, Bioconvection in Casson nanofluid flow with Gyrotactic microorganisms and variable surface heat flux, Int. J. Biomath. 12 (04) (2019) 1950041.